Computer Assisted Mechanics and Engineering Sciences, 14: 219–242, 2007.

Back analysis of microplane model parameters using soft computing methods

Anna Kučerová, Matěj Lepš, Jan Zeman
Department of Mechanics, Faculty of Civil Engineering, Czech Technical University in Prague
Thákurova 7, 166 29 Prague 6, Czech Republic

(Received in the final form March 20, 2007)

A new procedure based on layered feed-forward neural networks for the microplane material model parameters identification is proposed in the present paper. Novelties are usage of the Latin Hypercube Sampling method for the generation of training sets, a systematic employment of stochastic sensitivity analysis and a genetic algorithm-based training of a neural network by an evolutionary algorithm. Advantages and disadvantages of this approach together with possible extensions are thoroughly discussed and analyzed.

1. Introduction

Concrete is one of the most frequently used materials in Civil Engineering. Nevertheless, as a highly heterogeneous material, it shows very complex non-linear behavior, which is extremely difficult to describe by a sound constitutive law. As a consequence, numerical simulation of response of complex concrete structures still remains a very challenging and demanding topic in engineering computational modeling.

One of the most promising approaches to modeling of concrete behavior is based on the microplane concept, see, e.g., [7, Chapter 25] for general exposition and [1] for the most recent version of this family of models. It leads to a fully three-dimensional material law that incorporates tensional and compressive softening, damage of the material, supports different combinations of loading, unloading and cyclic loading along with the development of damage-induced anisotropy of the material. As a result, the M4 variant of the microplane model introduced in [2] is fully capable of predicting behavior of real-world concrete structures once provided with proper input data, see [8, 9] for concrete engineering examples. The major disadvantages of this model are, however, a large number of phenomenological material parameters and a high computational cost associated with structural analysis even in a parallel implementation [10]. Although the authors of the model proposed a heuristic calibration procedure [2, Part II], it is based on the trial-and-error method and provides only a rude guide for determination of selected material parameters. Therefore, a reliable and inexpensive procedure for the identification of these parameters is on demand.

In the view of potential improvements demonstrated in the recent work by Novák and Lehký [12], the applicability of a novel procedure based on artificial neural networks (ANN's) for the microplane parameter identification is examined in the present contribution. Individual steps of the identification procedure involve (see also Fig. 1 and [12, 14] for more details)

Step 1 *Setup of* a virtual and/or real experimental *test* used for the identification procedure.

Step 2 Formulation of an appropriate computational model. *Input data* to the model coincide with the parameters to be identified.

Step 3 *Randomization* of input parameters. Input data are typically assumed to be random variables uniformly distributed on a given interval.

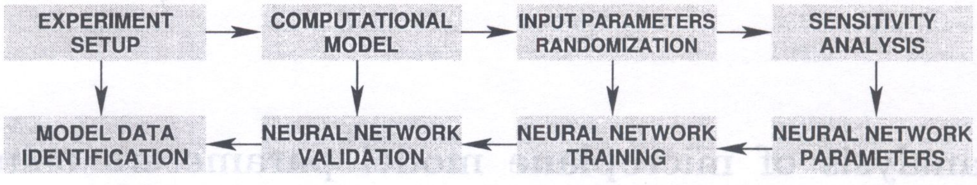
EXPERIMENT SETUP
COMPUTATIONAL MODEL
INPUT PARAMETERS RANDOMIZATION
SENSITIVITY ANALYSIS
MODEL DATA IDENTIFICATION
NEURAL NETWORK VALIDATION
NEURAL NETWORK TRAINING
NEURAL NETWORK PARAMETERS

Fig. 1. Flowchart of the inverse analysis procedure

Step 4 Stochastic *sensitivity analysis* using the Monte Carlo-based simulation. This provides us with *relevant model parameters* which can be reliably identified from the computational simulation.

Step 5 Definition of *topology* of an ANN used for the identification procedure.

Step 6 *Training* of the ANN. The training set is formed from the data generated during the sensitivity analysis step.

Step 7 *Validation* of the ANN with respect to the computational model. This step is usually performed by comparing the prediction of the ANN with an independent set of input data[1].

Step 8 The identification of relevant model parameters using trained ANN from available *experimental data*.

In the rest of the paper a more detailed description of the individual steps when applied to the microplane M4 model is presented. The basic outline of the constitutive model together with numerical solution scheme are presented in Section 2. The randomization of input parameters using small-sample Monte Carlo simulation is described in Section 3 together with stochastic sensitivity analysis. Section 4 is devoted to the procedure of ANN's training. The application to the identification of microplane model parameters is introduced in Section 5. Finally, the results obtained using the methodology are summarized in Section 6 together with comments on possible improvements.

2. Microplane model M4 for concrete

In contrary to traditional approaches to constitutive modeling, which build on description via second-order strain and stress *tensors* at individual points in the (x, y, z) coordinate system, the microplane approach builds the descriptions on planes of arbitrary spatial orientations – so-called *microplanes*, related to a macroscopic point, see Fig. 2. This allows to formulate constitutive equations in terms of stress and strain *vectors* in the coordinate system $(\mathbf{l}, \mathbf{m}, \mathbf{n})$ associated with a microplane oriented by a normal vector $\mathbf{n}$. The general procedure of evaluation of a strain-driven microplane model response for a given "macroscopic" strain tensor $\boldsymbol{\varepsilon}(\mathbf{x})$ can be described as follows: (i) for a given microplane orientation $\mathbf{n}$ normal "macroscopic" strain tensor $\boldsymbol{\varepsilon}(\mathbf{x})$ is projected onto the normal "microstrain" vector $\varepsilon(\mathbf{n})$ and the shear microstrains $\varepsilon(\mathbf{m})$ and $\varepsilon(\mathbf{l})$, (ii) the normal and shear microstresses $\sigma(\mathbf{n}), \sigma(\mathbf{m})$ and $\sigma(\mathbf{l})$ are evaluated using microplane constitutive relations, (iii) the "macroscopic" stress tensor $\boldsymbol{\sigma}(\mathbf{x})$ is reconstructed from the microscopic ones using the principle of virtual work, see, e.g., [7, Chapter 25] for more details. In the particular implementation, 28 microplanes with a pre-defined orientation on the unit hemisphere is used to evaluate the response of the model.

To close the microplane model description, the appropriate microplane constitutive relation must be provided to realistically describe material behavior. The model examined in the current work is the microplane model M4 [2]. The model uses volumetric-deviatoric split of the normal components of the stress and strain vectors, treats independently shear components of a microplane and introduces the concept of "boundary curves" to limit unrealistically high values predicted by

[1] usually called a "training set"

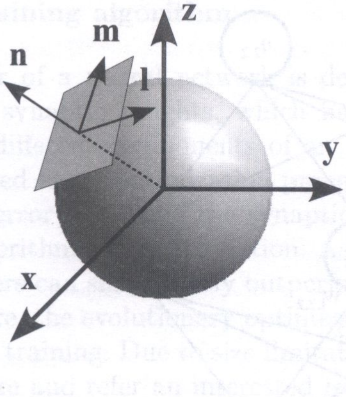

Fig. 2. Concept of microplane modeling

Table 1. Bounds for the microplane model parameters

Parameter		Bounds
E	$\in$	$\langle 20.0, 50.0\rangle$ GPa
ν	$\in$	$\langle 0.1, 0.3\rangle$
k_1	$\in$	$\langle 0.00008, 0.00025\rangle$
k_2	$\in$	$\langle 100.0, 1000.0\rangle$
k_3	$\in$	$\langle 5.0, 15.0\rangle$
k_4	$\in$	$\langle 30.0, 200.0\rangle$
c_3	$\in$	$\langle 3.0, 5.0\rangle$
c_{20}	$\in$	$\langle 0.2, 5.0\rangle$

earlier versions of the model. As a result, the strain-to-stress map $\boldsymbol{\varepsilon}(\mathbf{x}) \mapsto \boldsymbol{\sigma}(\mathbf{x})$ is no longer smooth, which complicates the formulation of consistent tangent stiffness matrix [10] and, subsequently, gradient-based approaches to material model parameters identification.

In overall, the microplane model M4 needs eight parameters to describe a certain type of concrete, namely: Young's modulus E, Poisson's ratio ν, and other six parameters (k_1 , k_2 , k_3 , k_4 , c_3 , c_{20}), which do not have a simple physical interpretation, and therefore it is difficult to determine their values from experiments. The only information available in the open literature are the bounds shown in the Table 1.

In the present work, the computational model of a structure is provided by the object-oriented C++ finite element code **OOFEM 1.5** [13]. Spatial discretization is performed using linear brick elements with eight integration points. The arc-length method with elastic stiffness matrix is used to determine the load–displacement curve related to the analyzed experiment.

3. Input parameter randomization and stochastic sensitivity analysis

The novelty of the identification approach proposed in [12] is a systematic use of small-sample Monte Carlo simulation method for generation of neural network training sets as well as stochastic sensitivity analysis. In the particular case of the M4 microplane model, each input parameter is assumed to be uniformly distributed on an interval specified in Table 1.

The Latin Hypercube Sampling (LHS) method [6] is used to generate particular realization of input variables as it enables to minimize the amount of simulations needed to reliably train a neural network. Moreover, the Simulated Annealing optimization method available in the software package FREET [11] is used to maximize the statistical independence among individual samples. The Pearson product moment correlation coefficient, defined as

$$cor = \frac{\sum(x_i - \bar{x})(y_i - \bar{y})}{\sqrt{\sum(x_i - \bar{x})^2 \sum(y_i - \bar{y})^2}}\,, \tag{1}$$

where $\bar{x}$ and $\bar{y}$ denote the expected values of random variables X and Y, is used as a sensitivity measure to investigate the influence of individual parameters to a structural response. Note that the correlation coefficient is normalized as $-1 \leq cor \leq 1$, where higher absolute values indicate statistical dependence of the random output variable Y on the random input variable X.

4. Artificial neural network

In this work, layered fully connected feed-forward neural networks with bias neurons (see, e.g, [15]) are used for the parameter identification, see Fig. 3.

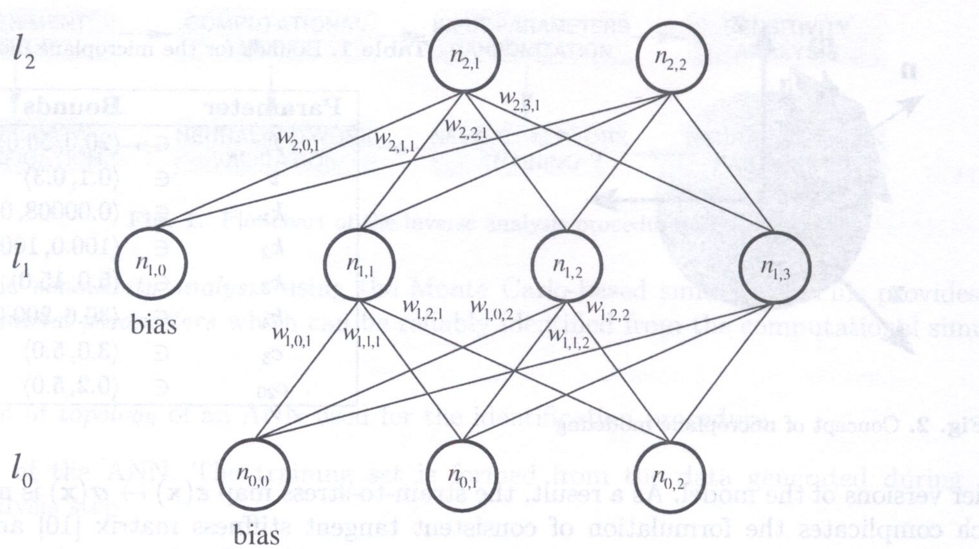

Fig. 3. Neural network architecture

In general, a neural network is created to map the input vector $I = (I_0, I_1, \dots I_m)$ on a target vector $T = (T_0\,, T_1\,, \dots T_n)$. There are L layers denoted as $l_0, l_1 \dots l_{L-1}$, where l_0 is the input layer and l_{L-1} is the output layer. The i-th layer l_i has N_i neurons denoted as $n_{i,1}\,, n_{i,2}\,, \dots n_{i,N_i}$. Each layer except the output layer has the bias neuron $n_{i,0}$. The connections are described by the weights $w_{l,i,j}$, where $l = 1, 2 \dots L-1$ denotes a layer, $i = 0, 1 \dots N_{l-1}$ is the index number of a neuron in the preceding layer $l-1$ ($i = 0$ for bias neurons) and $j = 1, 2 \dots N_l$ is the index number of a neuron in the layer l. The output of the neuron $n_{l,j}$ is then defined as

$$O_{l,j} = f_{\text{act}}\left(\sum_{i=0}^{N_{l-1}} O_{l-1,i} \cdot w_{l,i,j}\right), \qquad l = 1, 2 \dots L-1\,, \quad j = 1, 2 \dots N_l \tag{2}$$

$$O_{0,j} = I_j\,, \qquad j = 1, 2 \dots N_0\,, \tag{3}$$

$$O_{l,0} = 1, \qquad l = 0, 1 \dots L-1\,, \tag{4}$$

where f_{act} is an activation function. In our current implementation the activation function has the following form,

$$f_{\text{act}}(\Sigma) = \frac{1}{(1 + e^{-\alpha/\Sigma})}\,, \tag{5}$$

where α is the gain of the f_{act}. The value $\alpha = 0.5$ is used in all reported calculations. The output vector of each layer l_i is denoted as $O_i = (O_{i,1}\,, O_{i,2}\,, \dots O_{i,N_i})$. Finally, the neural network is propagated as follows:

1. Let $l = 1$.
2. Calculate $O_{l,i}$ for $i = 1, 2 \dots N_l$.
3. $l = l + 1$.
4. If $l < L$ go to 2, else O_{L-1} is the network's approximation of T.

The output error, which is used as a measure of a training level, is defined as

$$\varepsilon = \sqrt{\sum_{i=1}^{N_{L-1}} (T_i - O_{L-1,i})^2}\,. \tag{6}$$

4.1. Training algorithm

Behavior of a neural network is determined by a preceding training process. It consists of finding the synaptic weights, which have influence on the response of a neural network, depending on the different components of an input signal. The training of a neural network itself could be considered as an optimization process, because it can be seen as a minimization of neural network output error (6). Then the synaptic weights of a neural network act as variables of the optimization algorithm's fitness function. As it was shown earlier, e.g. in [3], evolutionary algorithm-based optimizers can significantly outperform the traditional methods, e.g. the back-propagation method. Therefore, the evolutionary optimization algorithm **GRADE**, proposed in [5], is used for the neural network training. Due to size limitations, we present only a sketchy description of the corresponding procedure and refer an interested reader to [4, 5] for a more elaborate discussion.

In the computations to follow we will work with the population of $10 \times n$ chromosomes, where n is the total number of unknowns in the problem. This population evolves through the following operations:

Mutation Let $\mathbf{x}_i(g)$ be the i-th chromosome in a generation g,

$$\mathbf{x}_i(g) = (x_{i1}(g)\,,\, x_{i2}(g)\,,\, \ldots\,,\, x_{in}(g)), \tag{7}$$

where n is the number of variables of the objective function. If a certain chromosome $\mathbf{x}_i(g)$ is chosen to be mutated, a random chromosome RP is generated from the definition domain and a new one $\mathbf{x}_k(g+1)$ is computed using the following relation,

$$\mathbf{x}_k(g+1) = \mathbf{x}_i(g) + MR(RP - \mathbf{x}_i(g)). \tag{8}$$

Parameter MR is chosen randomly from the interval $(0, 1)$. The number of new chromosomes created by the mutation operator is defined by "radioactivity", which is a parameter of the algorithm, with a constant value set to 0.2 for all reported calculations.

Gradient cross-over The aim of the cross-over operator is to create as many new chromosomes as there were in the last generation. The operator creates new chromosome $\mathbf{x}_i(g+1)$ according to the following sequential scheme: choose randomly two chromosomes $\mathbf{x}_q(g)$ and $\mathbf{x}_r(g)$, compute their difference vector, multiply it by a coefficient CR and add it to the better one, i.e.

$$\mathbf{x}_i(g+1) = \max(\mathbf{x}_q(g); \mathbf{x}_r(g)) + SG \times CR\,(\mathbf{x}_q(g) - \mathbf{x}_r(g)). \tag{9}$$

The parameter CR is chosen randomly from the interval $(0, CL)$, where CL is a parameter of the algorithm equal to 1.0 for all our calculations. SG denotes the sign change parameter which is supposed to get the correct orientation of the increase with respect to the gradient of the objective function.

Selection represents the kernel of each genetic algorithm. The goal is to provide a progressive improvement of the whole population, which is achieved by reducing the number of the "living" chromosomes together with conservation of the better ones. Modified tournament strategy is used for this purpose: two chromosomes are chosen randomly from a population, they are compared and the worse of them is cast off. This conserves population diversity thanks to a good chance of survival even for badly performing chromosomes.

Moreover, sometimes the method is "caught" in a local extreme and has no chance to escape unless a mutation randomly finds a sub-area with better values. If the gradient optimization methods are applied, this case is usually resolved by so-called *multi-start* principle. It consists of restarting the algorithm many times with different starting points. Similarly, any type of an evolutionary algorithm could be restarted many times. Nevertheless, the experience shows that there are functions with so-called deceptive behavior (and the training of a neural network is one of them), characterized by a high probability that the restarted algorithm would fall again into the same local extreme rather than explore another sub-area.

As a solution, the CERAF[2] method has been introduced in [4]. It produces areas of higher level of "radioactivity" in the neighborhood of all previously found local extremes by substantially increasing the mutation probability in these areas (this probability is set to 100% hereafter). The diameter of the radioactivity area (finally it defines a n-dimensional hyper-ellipsoid for all variables) is set to a 75% percentage of an appropriate variable interval. The time of stagnation that precedes the markup of a local extreme is a parameter of the method set to 100 generations. Similarly to the living nature, the radioactivity in the CERAF method is not constant in time but decreases during the time as the solutions produced by the cross-over are trying to get inside the radioactivity area, see again [4] for more details. When the number of stagnating generations is determined (the change between two best solutions in following generations is less than some very small value, $5 \cdot 10^{-11}$ in our case), the actual best solution is declared as the center of the new radioactive area and the whole population is restarted.

5. Identification of microplane model M4 parameters

The present section summarizes the individual steps of M4 material model identification. Following the heuristic calibration procedure suggested in [2, Part II], we examine three specific experimental tests: (i) uniaxial compression, (ii) hydrostatic test and (iii) triaxial test. Advantage of these tests is their simplicity and availability in most experimental facilities. Moreover, authors in [2] claim that these experiments are sufficient to determine all parameters of the microplane model M4. The results presented in this section can be understood as a verification of this claim.

5.1. Uniaxial compression test

The most common experiment used for the determination of concrete parameters is the uniaxial compression test on cylindrical concrete specimens. In particular, the cylinder with a radius equal to 75 mm and the height of 300 mm is used. The set-up of the experiment, the finite element mesh as well as the deformed configuration predicted by the computational model are shown in Fig. 4.

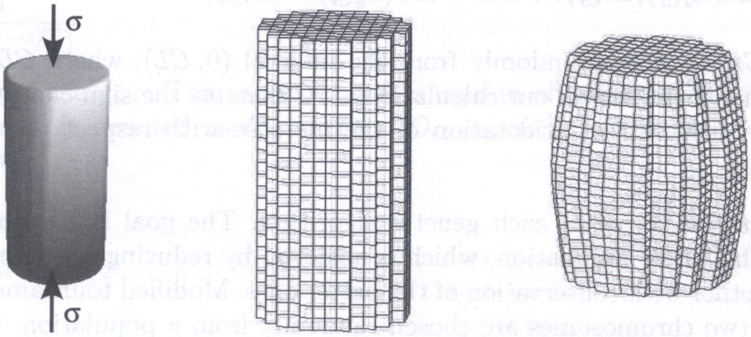

Fig. 4. Uniaxial test: (a) experiment setup, (b) finite element mesh, (c) deformed mesh

[2] Abbreviation of the French expression *CEntre RAdioactiF* – the radioactivity center.

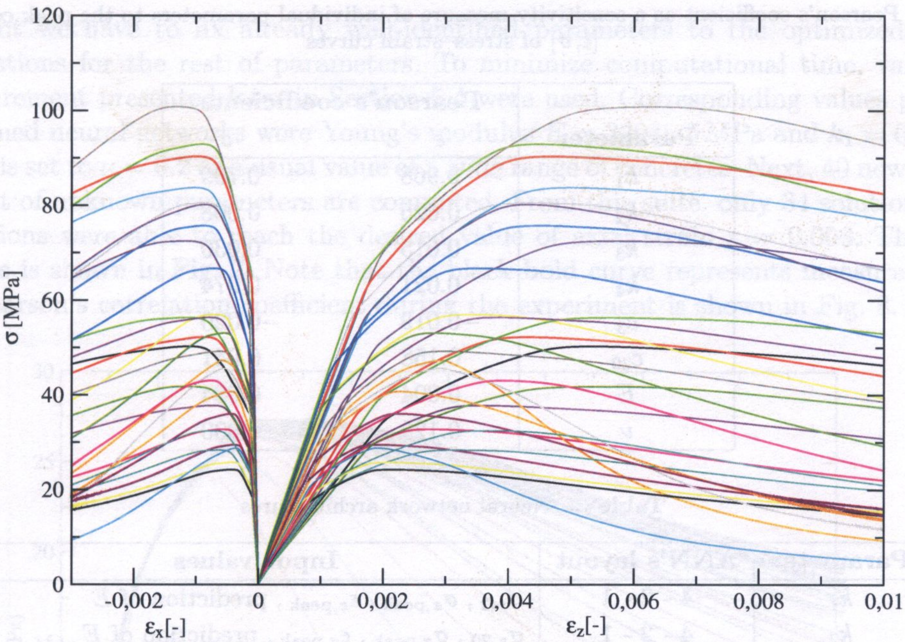

Fig. 5. Bundle of simulated stress–strain curves for uniaxial compression test

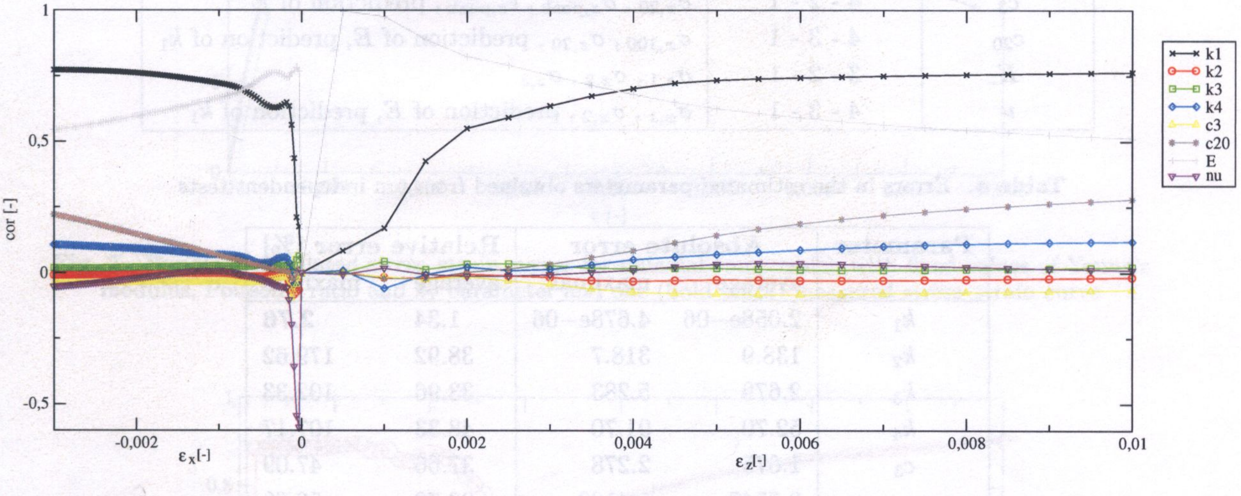

Fig. 6. Sensitivity evolution for uniaxial compression test

The LHS sampling procedure has been used to determine the set of 30 simulations resulting in a "bundle" of stress–strain curves shown in Fig. 5. The evolution of stochastic sensitivity during the loading process is depicted in Fig. 6. The results indicate that the most sensitive parameters are Young's modulus E, the coefficient k_1, Poisson's ratio ν (especially for the initial stages of loading) and, for the later stages of loading, the coefficient c_{20}. Therefore, one can expect that only these parameters can be reliably identified from this test.

Moreover, the impact of individual parameters on a position of a peak of stress–strain curves is computed. The results of a sensitivity analysis using Pearson's product moment correlation coefficient of peak coordinates $[\epsilon, \sigma]$ are listed in Table 2. Results indicate particularly strong influence of the k_1 parameter, which hopefully allows its reliable determination.

Based on the results of sensitivity analysis, the neural network training can be performed using a nested strategy. First, *Young's modulus* E with sensitivity ≈ 1 in the initial stage is easily identified. To this end, a three-layer ANN is used. In the first layer only the neurons corresponding to the values of stresses $\sigma_{z,1}$, $\sigma_{z,2}$ and $\sigma_{z,3}$ in the first three points of axial strain with extremal

Table 2. Pearson's coefficient as a sensitivity measure of individual parameters to the peak coordinates $[\epsilon, \sigma]$ of stress–strain curves

Parameter	Pearson's coefficients	
	ϵ	σ
k_1	0.968	0.709
k_2	0.025	0.008
k_3	0.015	0.030
k_4	0.021	0.074
c_3	−0.019	−0.020
c_{20}	0.158	0.041
E	0.004	0.684
ν	0.129	0.000

Table 3. Neural network architectures

Parameter	ANN's layout	Input values
k_1	4 - 2 - 1	$\sigma_{x,2}$, $\sigma_{z,\mathrm{peak}}$, $\epsilon_{z,\mathrm{peak}}$, prediction of E
k_2	4 - 2 - 1	$\sigma_{z,20}$, $\sigma_{z,\mathrm{peak}}$, $\epsilon_{z,\mathrm{peak}}$, prediction of E
k_3	4 - 2 - 1	$\sigma_{z,20}$, $\sigma_{z,\mathrm{peak}}$, $\epsilon_{z,\mathrm{peak}}$, prediction of E
k_4	4 - 2 - 1	$\sigma_{z,20}$, $\sigma_{z,\mathrm{peak}}$, $\epsilon_{z,\mathrm{peak}}$, prediction of E
c_3	4 - 2 - 1	$\sigma_{z,20}$, $\sigma_{z,\mathrm{peak}}$, $\epsilon_{z,\mathrm{peak}}$, prediction of E
c_{20}	4 - 3 - 1	$\sigma_{x,100}$, $\sigma_{z,20}$, prediction of E, prediction of k_1
E	3 - 2 - 1	$\sigma_{z,1}$, $\sigma_{z,2}$, $\sigma_{z,3}$
ν	4 - 3 - 1	$\sigma_{x,1}$, $\sigma_{x,2}$, prediction of E, prediction of k_1

Table 4. Errors in the estimated parameters obtained from ten independent tests

Parameter	Absolute error		Relative error [%]	
	average	maximal	average	maximal
k_1	2.058e−06	4.678e−06	1.34	**2.76**
k_2	138.9	318.7	38.92	179.62
k_3	2.679	5.283	33.96	102.33
k_4	52.70	91.70	48.33	107.17
c_3	1.675	2.278	37.66	47.09
c_{20}	0.7547	1.4168	26.70	56.69
E	229.3	594.5	0.74	**1.79**
ν	0.006447	0.010361	2.93	**4.72**

Pearson's correlation coefficient are chosen. The second layer contains two neurons only; the last layer consists of one neuron corresponding to the predicted value of Young's modulus E. For the ANN training the GRADE algorithm is used and calculation is stopped after 1 000 000 iterations of the algorithm.

The three-layer ANN trained using the **GRADE** algorithm is also used for the identification of other microplane model parameters. In Table 3 network's architectures and the choice of input values for the identification of each microplane parameter are presented.

The results of the identification for an independent set of ten stress–strain curves using the proposed strategy are shown in Table 4.

Note that obtained errors are in a close agreement with the results of sensitivity analysis. Except E, ν and k_1, the parameters of the model are identified with very high error values. Therefore, additional simulations are needed to obtain these values reliably.

At this point we have to fix already well-identified parameters to the optimized values and perform simulations for the rest of parameters. To minimize computational time, values for one uniaxial measurement presented later in Section 5.4 were used. Corresponding values predicted by previously learned neural networks were Young's modulus $E = 32035.5$ MPa and $k_1 = 0.000089046$. Poisson's ratio is set to $\nu = 0.2$ as a usual value of a wide range of concretes. Next, 40 new simulations varying the rest of unknown parameters are computed. From this suite, only 34 solutions are valid, i.e. these solutions were able to reach the desired value of axial strain $\varepsilon = 0.008$. The bundle of resulting curves is shown in Fig. 7. Note that the black bold curve represents measured data. The evolution of Pearson's correlation coefficient during the experiment is shown in Fig. 8.

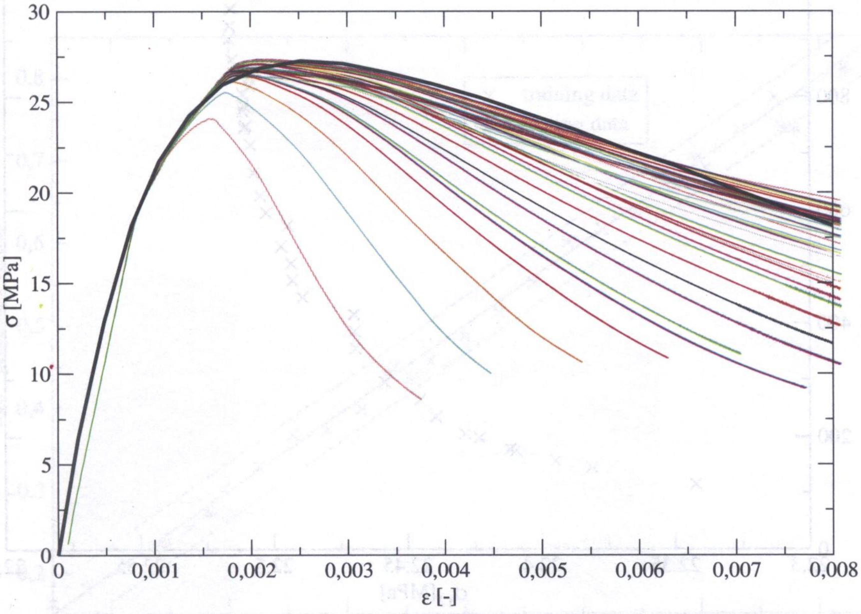

Fig. 7. Bundle of simulated stress–strain curves for uniaxial compression with fixed values of Young's modulus, Poisson's ratio and k_1 parameter and one (bold black) measured stress–strain curve

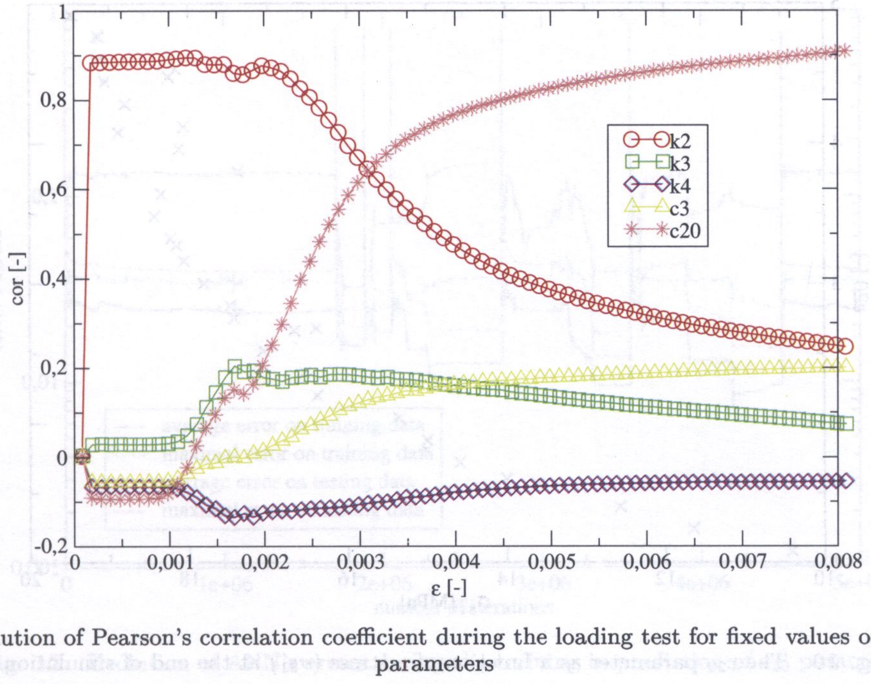

Fig. 8. Evolution of Pearson's correlation coefficient during the loading test for fixed values of E, ν and k_1 parameters

The sensitivity shows very high influence of k_2 parameter at the beginning of the loading. If we inspect Fig. 9, it is clear that the k_2 parameter influences the stress–strain curve only on a very narrow interval and hence the parameter k_2 cannot be identified from this test (the authors of the microplane model indeed proposed k_2 to be estimated from the triaxial compression test). We are more interested in fitting data in the post-peak part. For post-peak curves, sensitivity analysis shows especially growing influence of c_{20} parameter. This can be demonstrated by a relation between the c_{20} parameter and a value of a stress (σ_{81}) at the end of our simulations, where the correlation coefficient reaches the value 0.904429. This relation is graphically illustrated in Fig. 10.

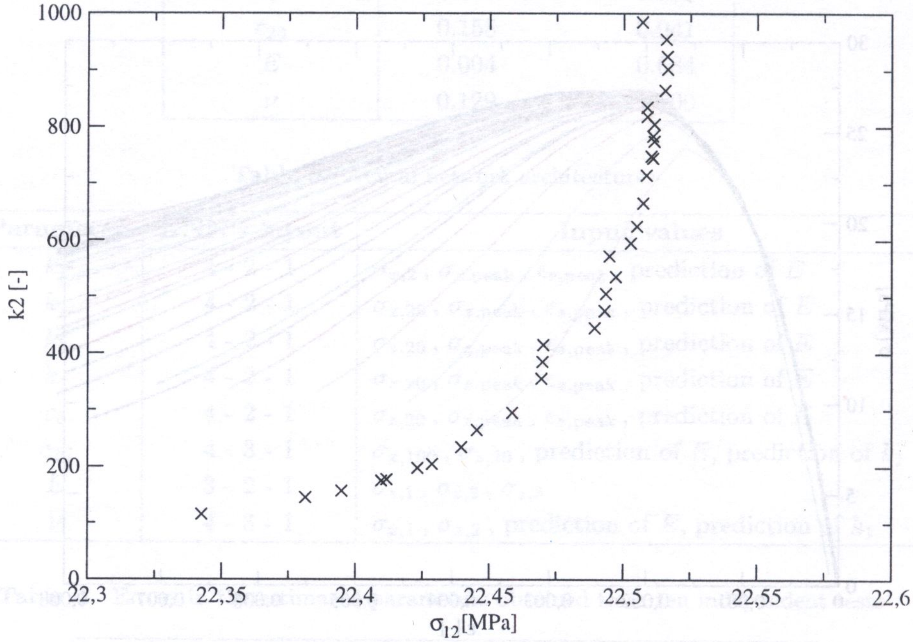

Fig. 9. k_2 parameter as a function of the stress σ_{12} (corresponding to $\epsilon = 0.0011$)

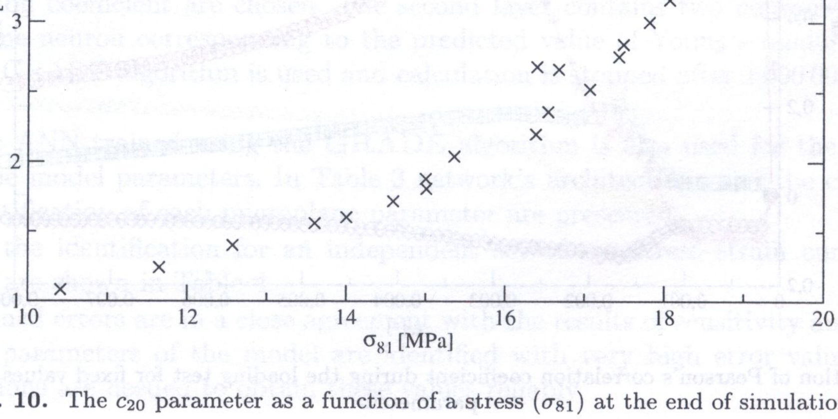

Fig. 10. The c_{20} parameter as a function of a stress (σ_{81}) at the end of simulations

It is clearly visible that this relation is not highly non-linear and any simple regression of this data is not possible. We applied the ANN with 3 input neurons chosen to get the best prediction of parameters based on post-peak curves. Therefore, one input value is a stress value at the peak σ_{peak} and the other two inputs are stress values σ_{61} and σ_{81} corresponding to strains $\epsilon = 0.006$ and $\epsilon = 0.008$, respectively. Two neurons in the hidden layer were used. Quality of ANN prediction is demonstrated in Fig. 11. In particular, the exact prediction of the searched value corresponds to a point lying on the the axis of the first quadrant. Values of predicted parameters are normalized here to the interval $\langle 0.15, 0.85\rangle$. Dashed parallel lines bound a 5% relative error related to the size of the parameter's interval. Clearly, the identification procedure works with an error which does not exceed the chosen 5% tolerance.

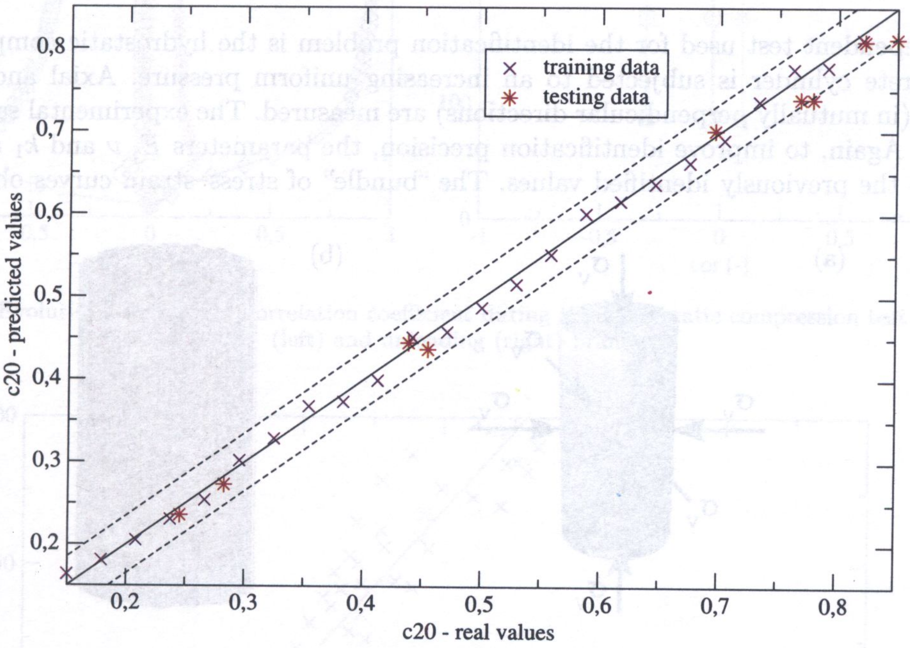

Fig. 11. Quality of ANN predictions of c_{20} parameter

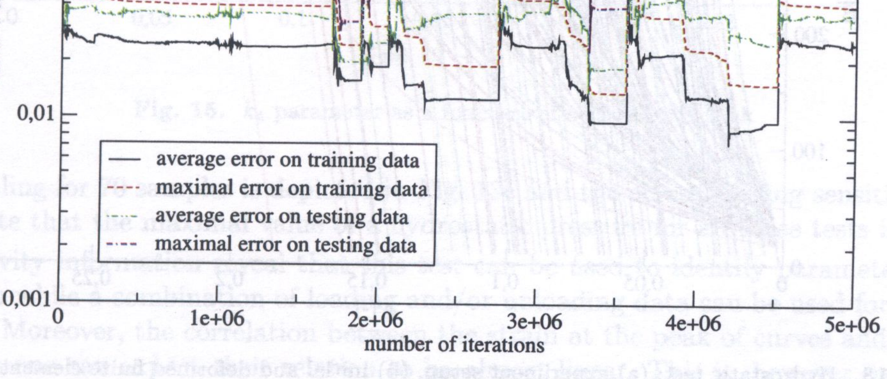

Fig. 12. Evolution of ANN's errors during the training in prediction of c_{20} parameter

The attention is also paid to the over-training of the ANN. To control this aspect, the evolution of errors in ANN's predictions during the training process on the training and testing data are monitored (see Fig. 12). Recall that if the errors on the testing set are much higher than on the training set, we suppose such an ANN to be over-trained. Even though this seems to be the case of the current ANN, we attribute such a behavior to the fact that there are more training data (in our case 25) than 11 neural weights optimized by the algorithm. Also note the typical restarting of the optimization process caused by the multi-modal optimization strategy CERAF presented in Section 4.1.

5.2. Hydrostatic test

The next independent test used for the identification problem is the hydrostatic compression test, where a concrete cylinder is subjected to an increasing uniform pressure. Axial and two lateral deformations (in mutually perpendicular directions) are measured. The experimental setup is shown in Fig. 13a,b. Again, to improve identification precision, the parameters E, ν and k_1 are supposed to be fixed to the previously identified values. The "bundle" of stress–strain curves obtained using

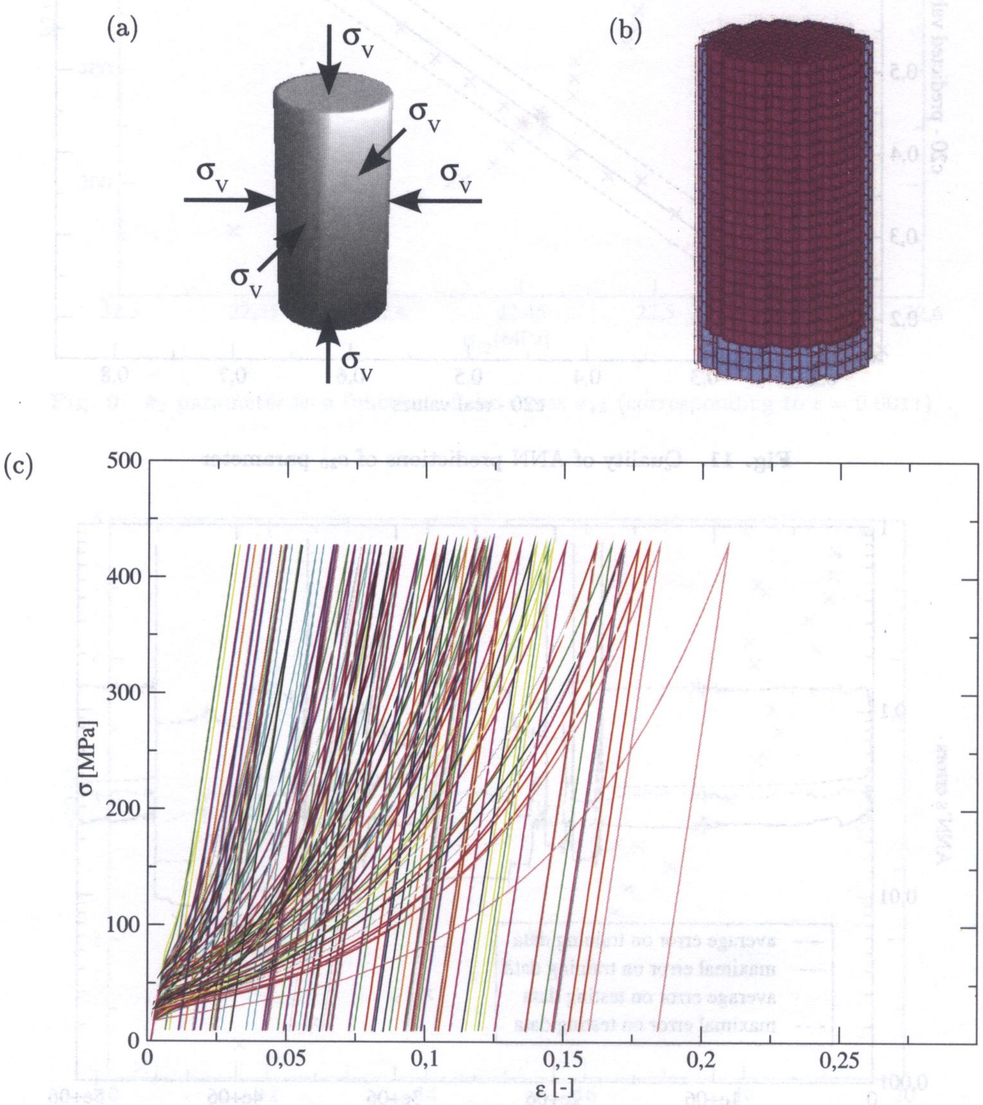

Fig. 13. Hydrostatic test: (a) experiment setup, (b) initial and deformed finite element mesh, (c) stress–strain curves

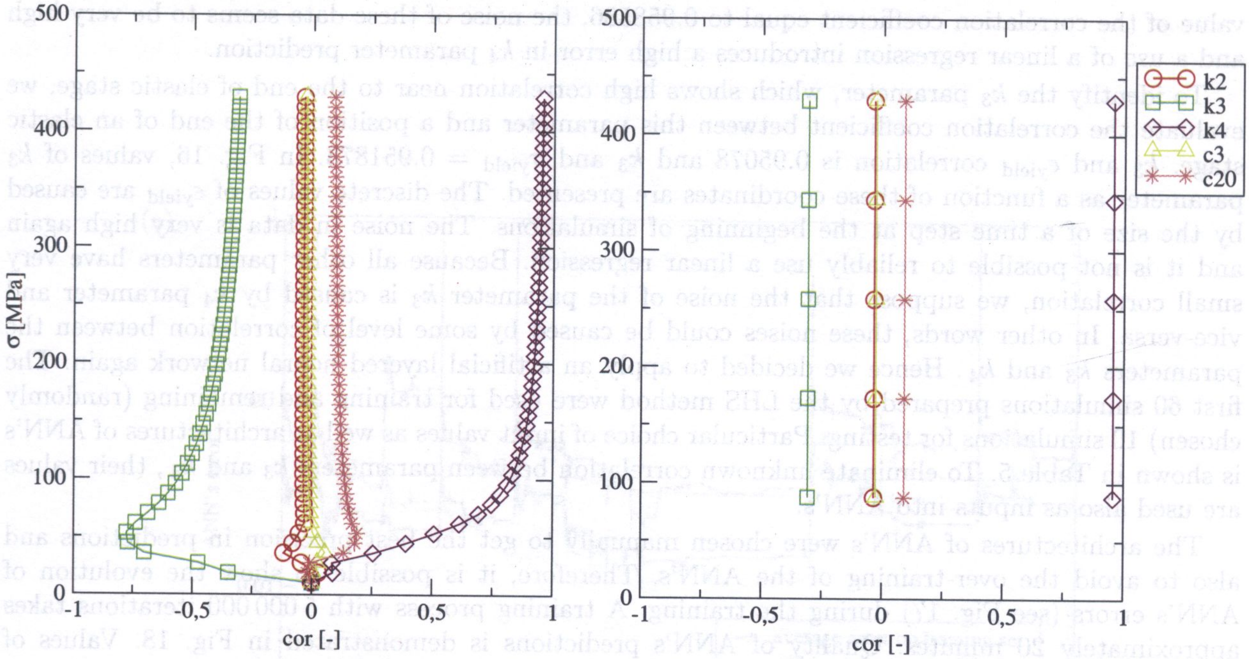

Fig. 14. Evolution of Pearson's correlation coefficient during the hydrostatic compression test for loading (left) and unloading (right) branch

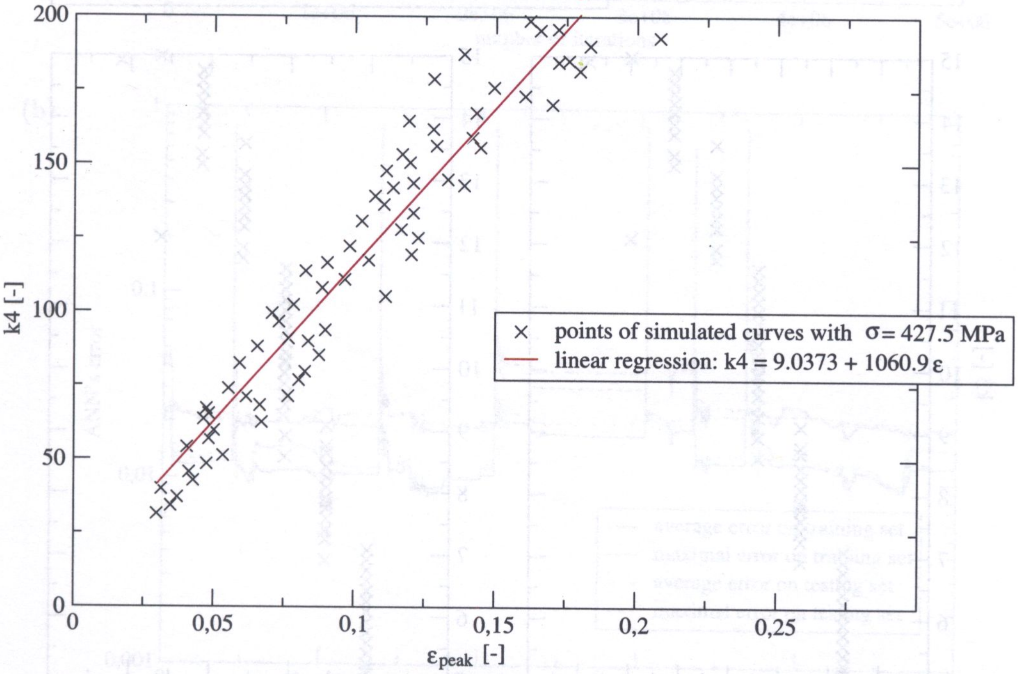

Fig. 15. k_4 parameter as a function of a strain of a peak

the LHS sampling for 70 samples is depicted in Fig. 13c and the corresponding sensitivity evolution in Fig. 14. Note that the maximal value of a hydrostatic pressure for all these tests is 427.5 MPa.

The sensitivity information reveal that this test can be used to identify parameter k_3 from the loading branch while a combination of loading and/or unloading data can be used for k_4 parameter identification. Moreover, the correlation between the strain at the peak of curves and k_4 parameter is so high that one can expect their relation to be almost linear. This is, however, not the case as illustrated by Fig. 15 showing the value of k_4 parameter as a function of a strain ε. In spite of a high value of the correlation coefficient equal to 0.958586, the noise of these data seems to be very high and a use of a linear regression introduces a high error in k_4 parameter prediction.

To identify the k_3 parameter, which shows high correlation near to the end of elastic stage, we evaluate the correlation coefficient between this parameter and a position of the end of an elastic stage. k_3 and ϵ_{yield} correlation is 0.95078 and k_3 and $\sigma_{\text{yield}} = 0.951873$. In Fig. 16, values of k_3 parameter as a function of these coordinates are presented. The discrete values of ϵ_{yield} are caused by the size of a time step at the beginning of simulations. The noise in data is very high again and it is not possible to reliably use a linear regression. Because all other parameters have very small correlation, we suppose that the noise of the parameter k_3 is caused by k_4 parameter and vice-versa. In other words, these noises could be caused by some level of correlation between the parameters k_3 and k_4 . Hence we decided to apply an artificial layered neural network again. The first 60 simulations prepared by the LHS method were used for training and remaining (randomly chosen) 10 simulations for testing. Particular choice of input values as well as architectures of ANN's is shown in Table 5. To eliminate unknown correlation between parameters k_3 and k_4 , their values are used also as inputs into ANN's.

The architectures of ANN's were chosen manually to get the best precision in predictions and also to avoid the over-training of the ANN's. Therefore, it is possible to show the evolution of ANN's errors (see Fig. 17) during the training. A training process with 5 000 000 iterations takes approximately 20 minutes. Quality of ANN's predictions is demonstrated in Fig. 18. Values of predicted parameters are again normalized into the interval $\langle 0.15, 0.85\rangle$.

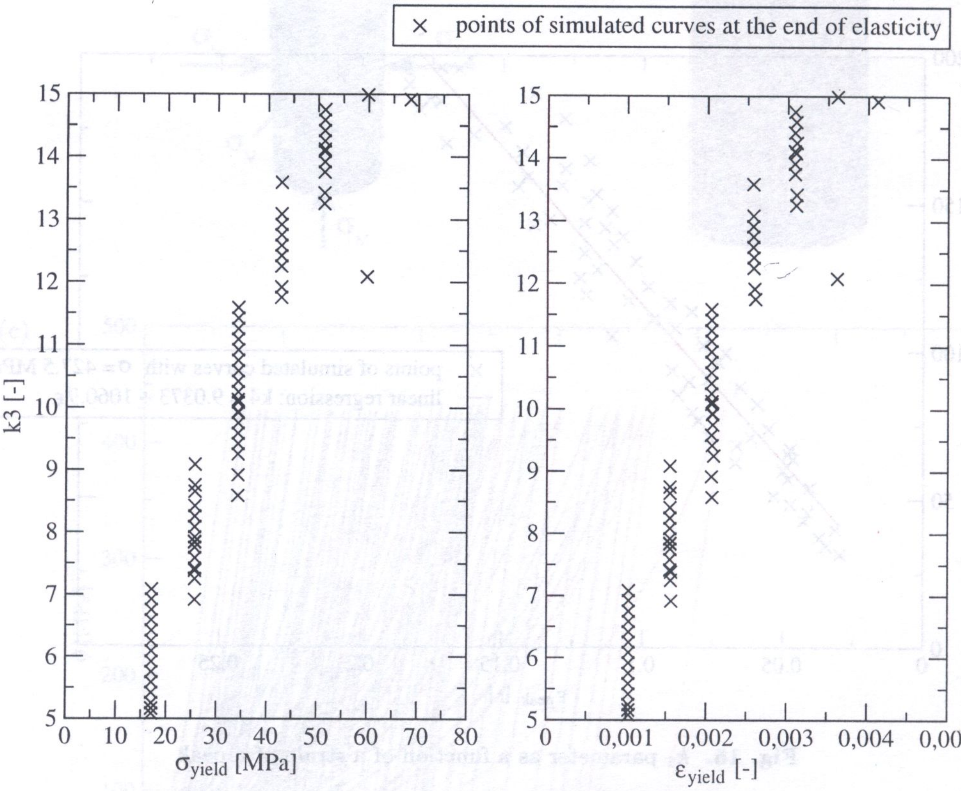

Fig. 16. k_3 parameter as a function of a position of the end of an elastic stage

Table 5. Neural network architectures for hydrostatic test

Parameter	ANN's layout	Input values
k_3	5 - 2 - 1	k_4 , ϵ_{yield} , $\epsilon_{\text{load},2}$, $\epsilon_{load,5}$, ϵ_{peak}
k_4	3 - 2 - 1	k_3 , ϵ_{peak} , $\epsilon_{\text{unload},4}$

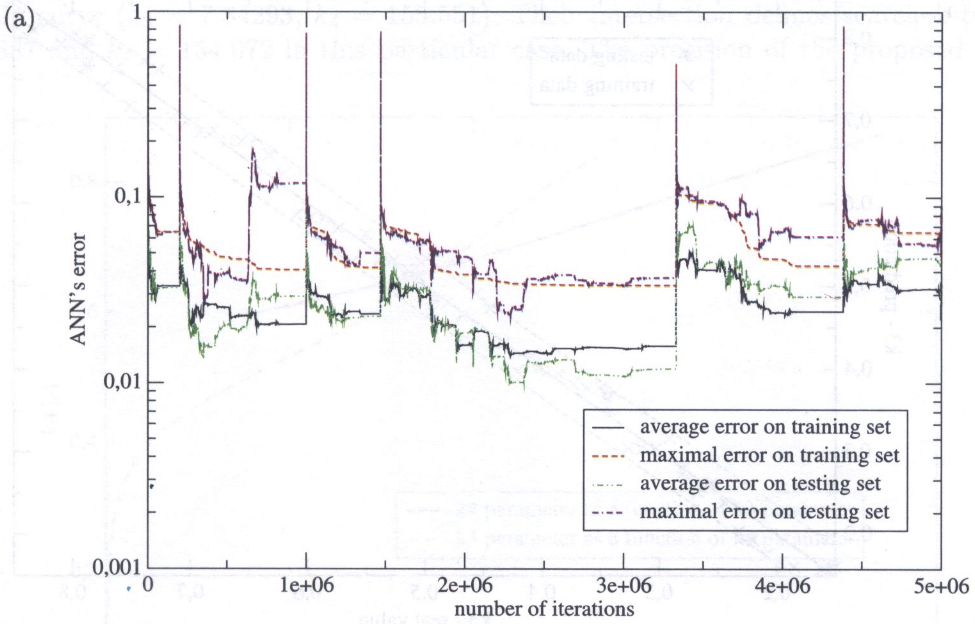

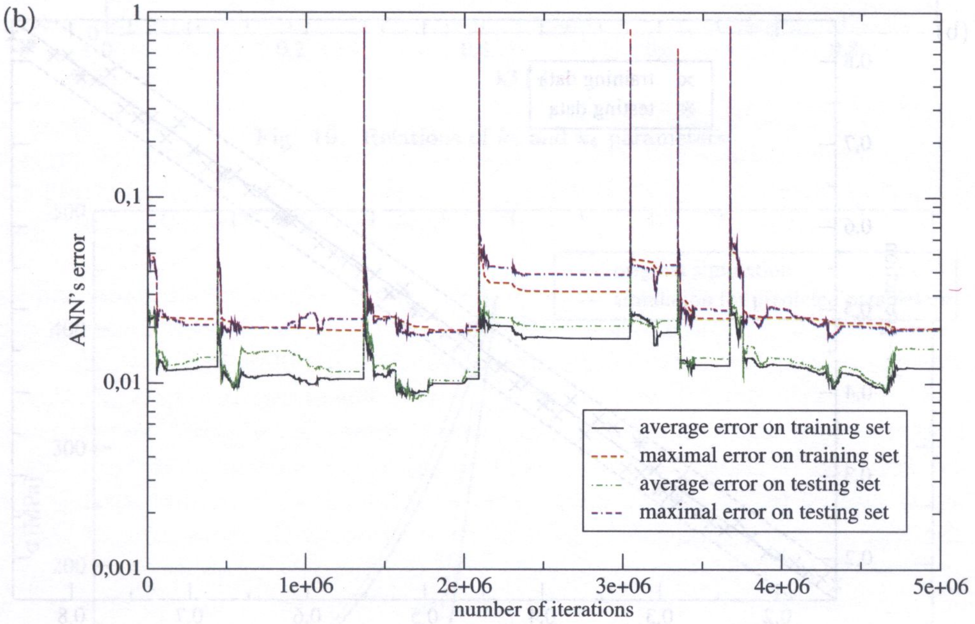

Fig. 17. Evolution of ANN's errors during the training process in prediction of (a) k_3 parameter and (b) k_4 parameter

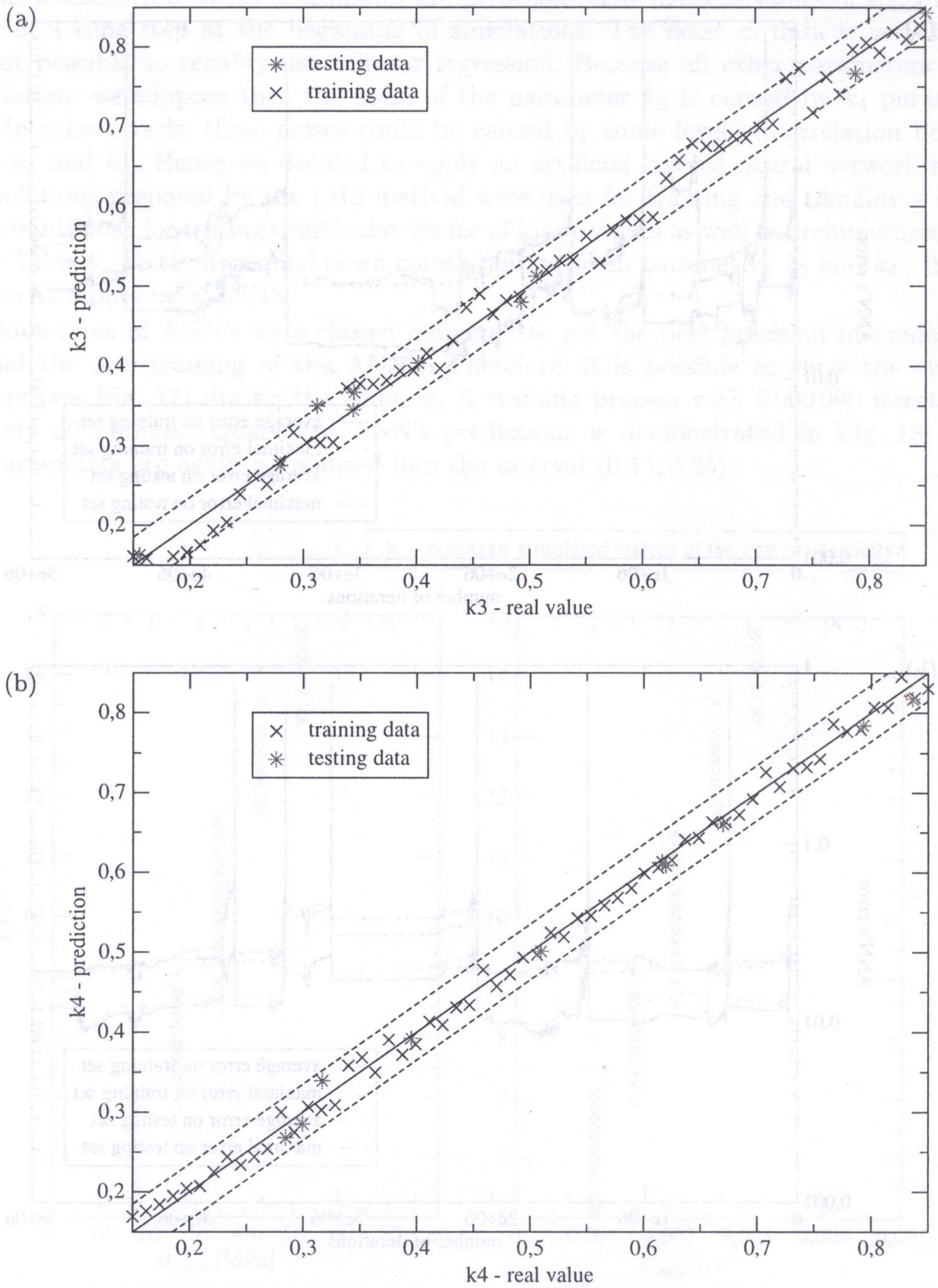

Fig. 18. Quality of ANN prediction of (a) k_3 parameter and (b) k_4 parameter

In this way, two ANN's or, in other words, two implicit functions are prescribed. One defines a value of k_3 parameter depending on a value of k_4 parameter and some other properties of a stress–strain curve, the second define a value of k_4 parameter depending on a value of k_3 parameter and some other properties of a stress–strain curve. Once we get some "measured" data and we fix all properties of a stress–strain curve, we get a system of two non-linear equations for k_3 and k_4. We can solve this system, e.g., graphically. Both relations are depicted in Fig. 19 for one independent stress–strain curve ($k_3 = 7.84293$, $k_4 = 155.551$). Their intersection defines searched parameters, $k_3 = 8.15687$ and $k_4 = 154.072$ in this particular case. The precision of the proposed strategy is

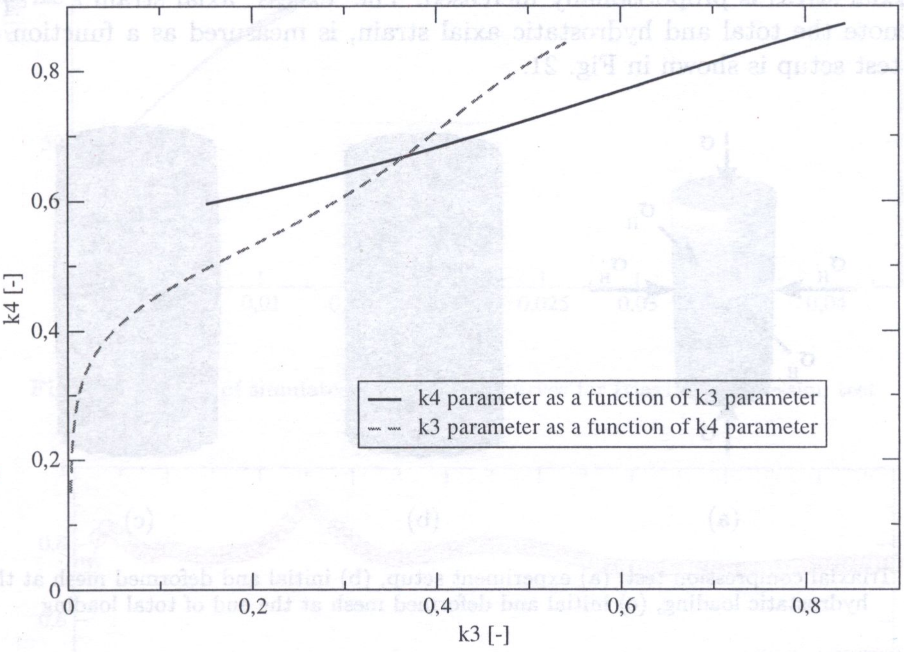

Fig. 19. Relations of k_3 and k_4 parameters

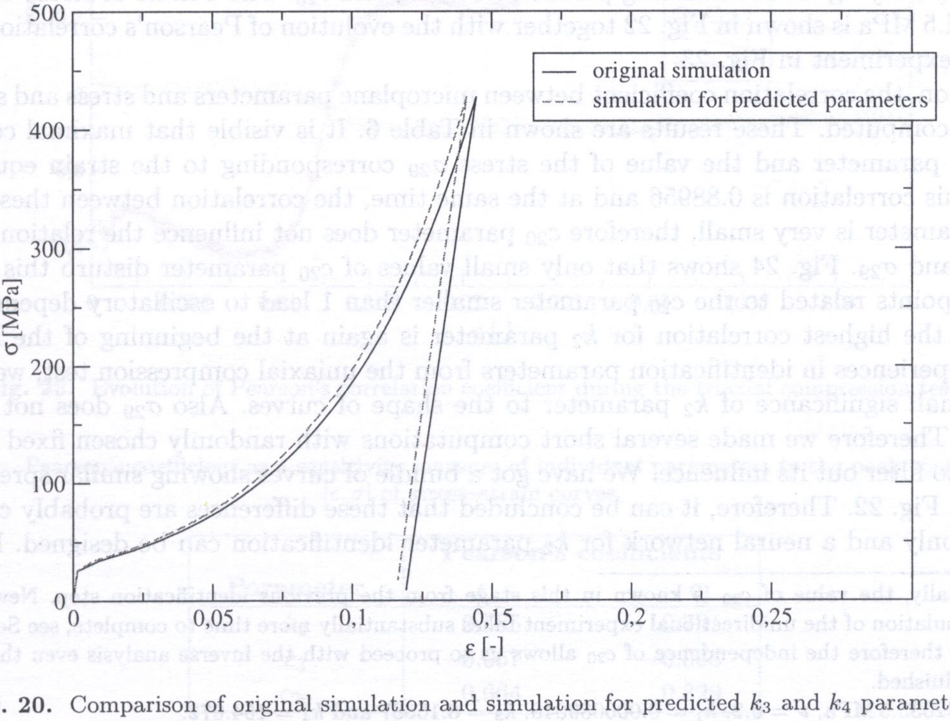

Fig. 20. Comparison of original simulation and simulation for predicted k_3 and k_4 parameters

visible in comparison of corresponding stress–strain curves, see Fig. 20. Note, that E, ν and k_1 were the same as in previous section and remaining parameters, i.e. k_2 , c_3 and c_{20} , were chosen randomly.[3]

5.3. Triaxial test

The last experiment, used for the purpose of parameter identification, is a triaxial compression test. To this end, a specimen is subjected to the hydrostatic pressure σ_H. After the peak value of σ_H is reached, the axial stress is proportionally increased. The "excess" axial strain $\varepsilon = \varepsilon_T - \varepsilon_H$, where ε_T and ε_H denote the total and hydrostatic axial strain, is measured as a function of the overall stress σ. The test setup is shown in Fig. 21.

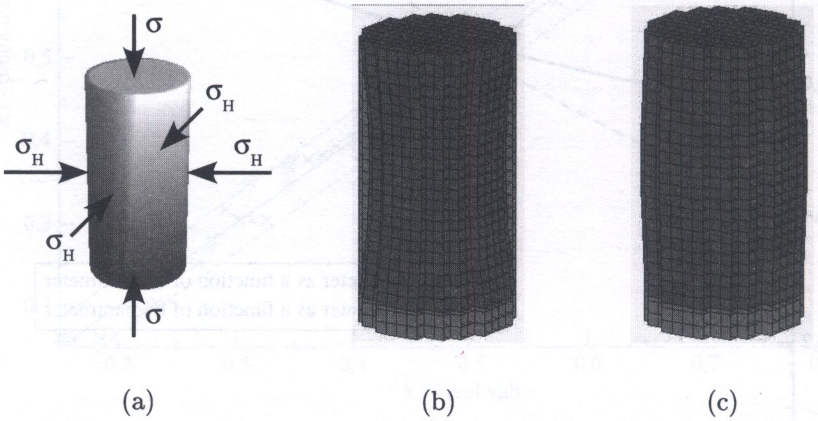

Fig. 21. Triaxial compression test: (a) experiment setup, (b) initial and deformed mesh at the end of hydrostatic loading, (c) initial and deformed mesh at the end of total loading

At this point, we assume that parameters E, ν, k_1 , k_3 and k_4 are known from previous identifications[4]. Next, 70 simulations (60 training and 10 testing) of the triaxial compression test are computed by varying three remaining parameters k_2, c_3 and c_{20}. The bundle of stress–strain curves for $\sigma_H = 34.5\,\mathrm{MPa}$ is shown in Fig. 22 together with the evolution of Pearson's correlation coefficient during the experiment in Fig. 23.

In addition, the correlation coefficient between microplane parameters and stress and strain values of peaks is computed. These results are shown in Table 6. It is visible that maximal correlation is between k_2 parameter and the value of the stress σ_{29} corresponding to the strain equal to $\epsilon_{29} = 0.01276$. This correlation is 0.88956 and at the same time, the correlation between these σ_{29} values and c_{20} parameter is very small, therefore c_{20} parameter does not influence the relation between k_2 parameter and σ_{29}. Fig. 24 shows that only small values of c_{20} parameter disturb this relation. In particular, points related to the c_{20} parameter smaller than 1 lead to oscillatory dependence.

Because the highest correlation for k_2 parameter is again at the beginning of the loading and after our experiences in identification parameters from the uniaxial compression test, we were again afraid of small significance of k_2 parameter to the shape of curves. Also σ_{29} does not seem to be significant. Therefore we made several short computations with randomly chosen fixed value of c_{20} parameter to filter out its influence. We have got a bundle of curves showing similar spread of values as curves in Fig. 22. Therefore, it can be concluded that these differences are probably caused by k_2 parameter only and a neural network for k_2 parameter identification can be designed. Because the

[3] Theoretically, the value of c_{20} is known in this stage from the previous identification step. Nevertheless, the numerical simulation of the unidirectional experiment takes substantially more time to complete, see Section 6 for an example, and therefore the independence of c_{20} allows us to proceed with the inverse analysis even though the first phase is not finished.

[4] i.e. $E = 32035.5\,\mathrm{MPa}$, $\nu = 0.2$, $k_1 = 0.000089046$, $k_3 = 8.15687$ and $k_4 = 154.072$.

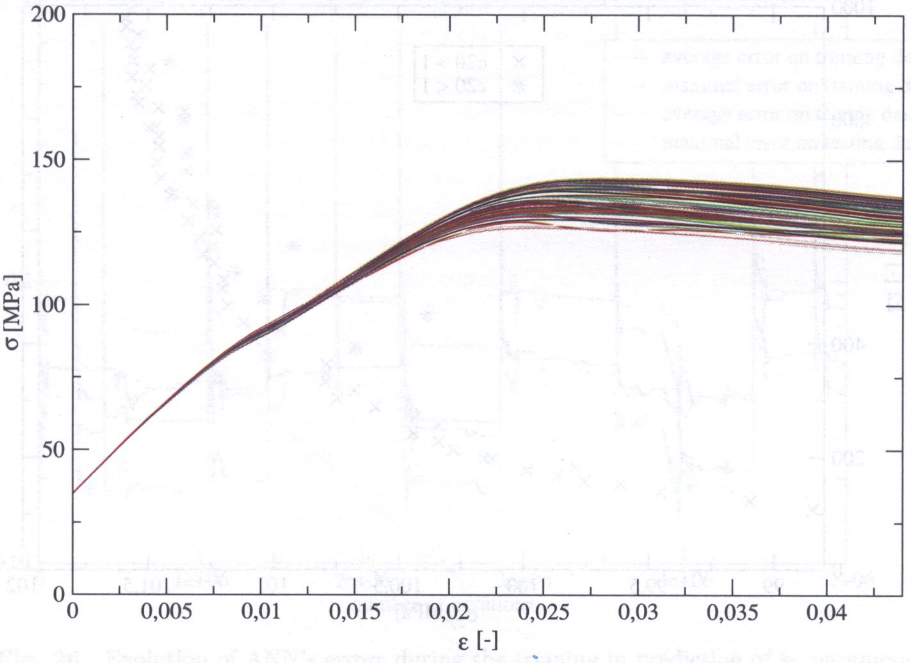

Fig. 22. Bundle of simulated stress–strain curves for triaxial compression test

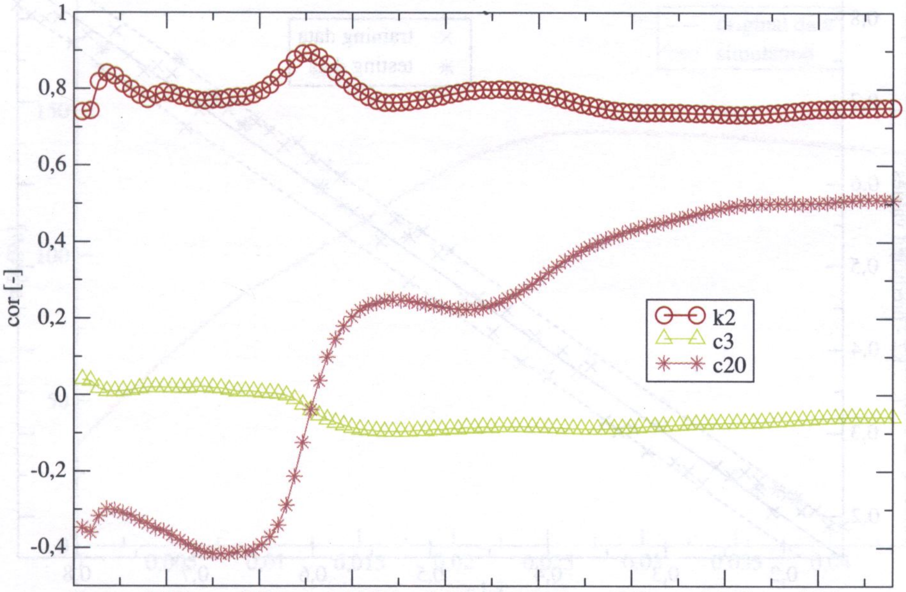

Fig. 23. Evolution of Pearson's correlation coefficient during the triaxial compression test

Table 6. Pearson's coefficient as a sensitivity measure of individual parameters to the peak coordinates $[\epsilon, \sigma]$ of stress–strain curves

Parameter	Pearson's coefficients	
	ϵ	σ
k_2	0.585	0.791
c_3	−0.067	−0.088
c_{20}	0.664	0.329

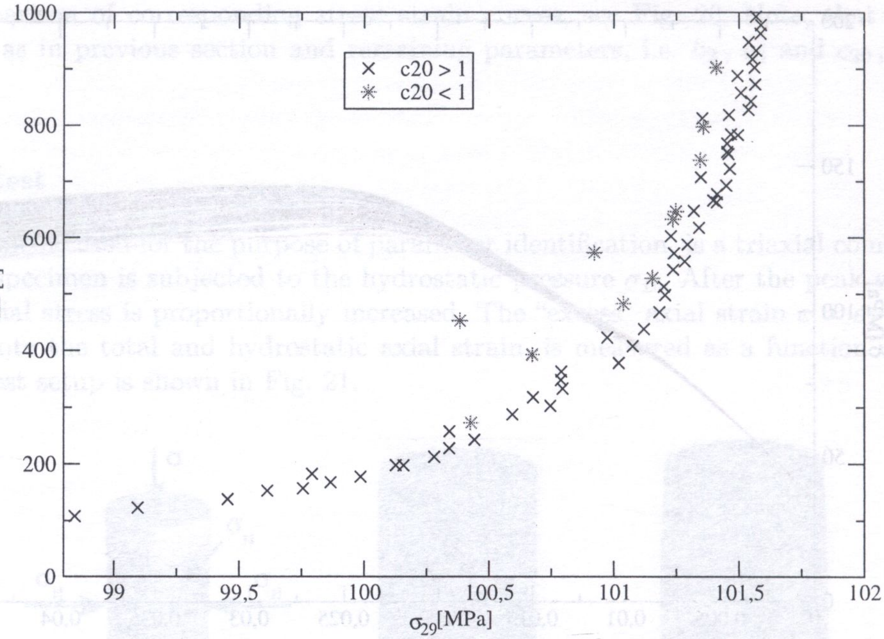

Fig. 24. k_2 parameter as a function of the stress value σ_{29}

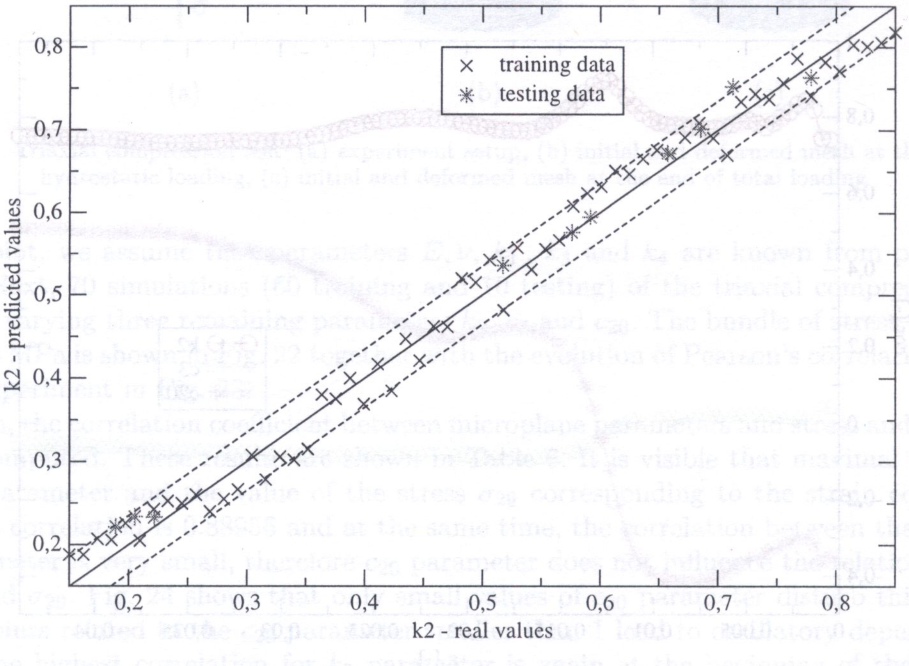

Fig. 25. Quality of ANN prediction of k_2 parameter.

bundle of curves varies mostly in the post-peak part and we would like to get a predictor capable to fit this part of a curve properly, we use σ_{peak} and σ_{100} as input values. The latter one correspond to the end of our simulations, where $\epsilon = 0.044$. We also add the third input value – σ_{29} – because of its small correlation with c_{20} parameter. Two neurons in the hidden layer were used. Quality of the ANN prediction is demonstrated in Fig. 25. Under- and over-fitting issues were again checked by errors evaluations during the training process, see Fig. 26.

Almost perfect precision of the proposed strategy is visible in comparison of corresponding stress–strain curves for $k_2 = 748.857$ and its prediction equal to 767.777 and randomly chosen parameters c_{20} and c_3 , see Fig. 27.

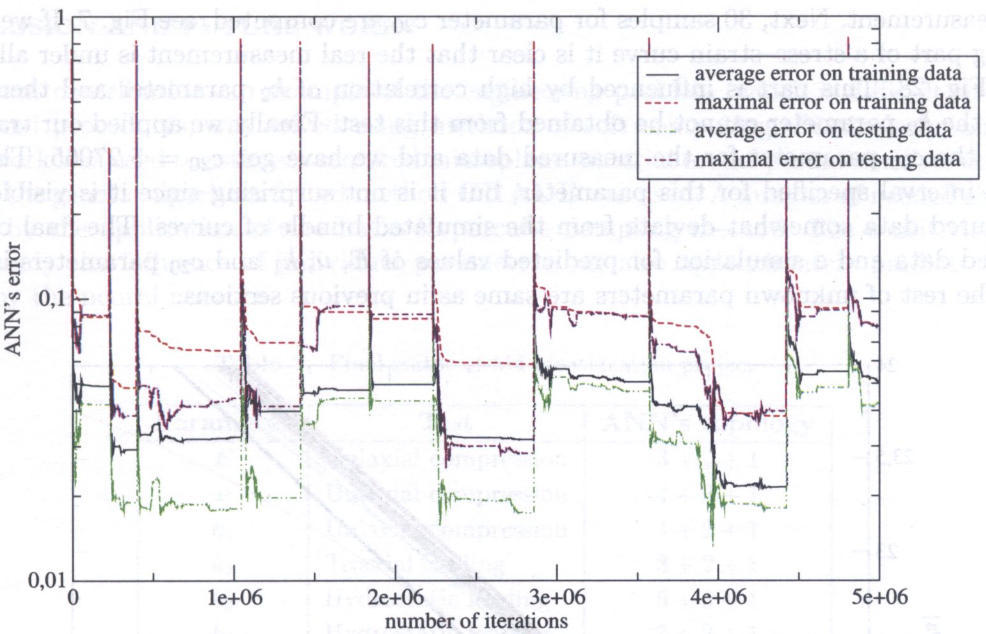

Fig. 26. Evolution of ANN's errors during the training in prediction of k_2 parameter

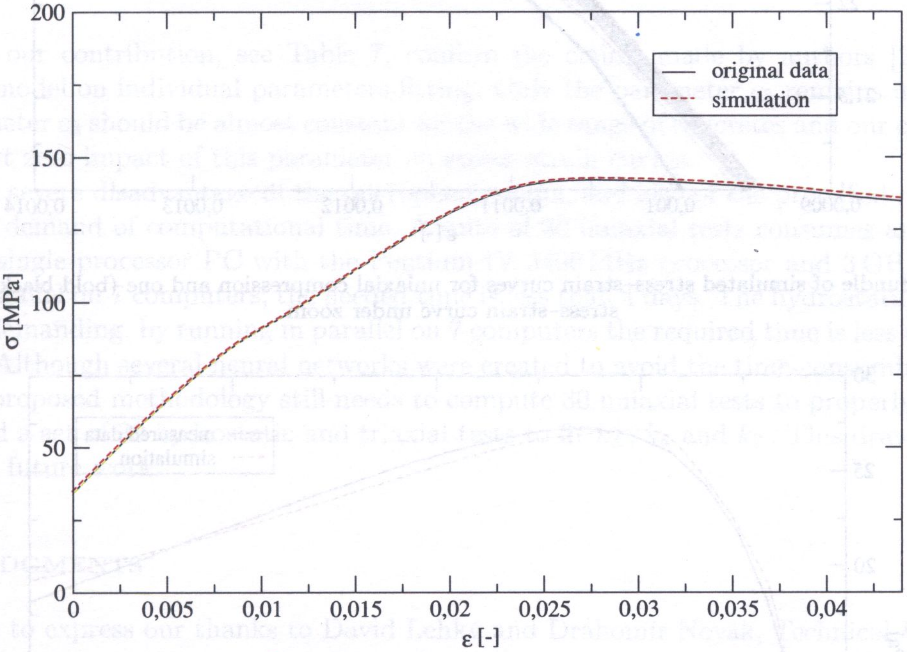

Fig. 27. Comparison of original simulation and simulation for predicted parameters of triaxial compression test

5.4. Application to measured data

In previous sections, we have shown that the proposed methodology is able to identify all but one (c_3) parameters from computer-simulated curves. To demonstrate the applicability of the proposed procedure, a real simulation should be examined. However, only limited experimental data from uniaxial compression tests are available to authors which leaves us with only one uniaxial stress–strain curve to be identified. As was mentioned previously in Section 5.1, Young's modulus $E = 32035.5$ MPa, Poisson's ratio $\nu = 0.2$ and $k_1 = 0.000089046$ are predicted by the neural network for this measurement. Next, 30 samples for parameter c_{20} are computed, see Fig. 7. If we zoom into the loading part of a stress–strain curve it is clear that the real measurement is under all simulated data, see Fig. 28. This part is influenced by high correlation of k_2 parameter and therefore, it is clear that the k_2 parameter cannot be obtained from this test. Finally we applied our trained ANN to predict the c_{20} parameter for the measured data and we have got $c_{20} = 5.27065$. This value is out of the interval specified for this parameter, but it is not surprising since it is visible in Fig. 7 that measured data somewhat deviate from the simulated bundle of curves. The final comparison of measured data and a simulation for predicted values of E, ν, k_1 and c_{20} parameters is shown in Fig. 29. The rest of unknown parameters are same as in previous sections.

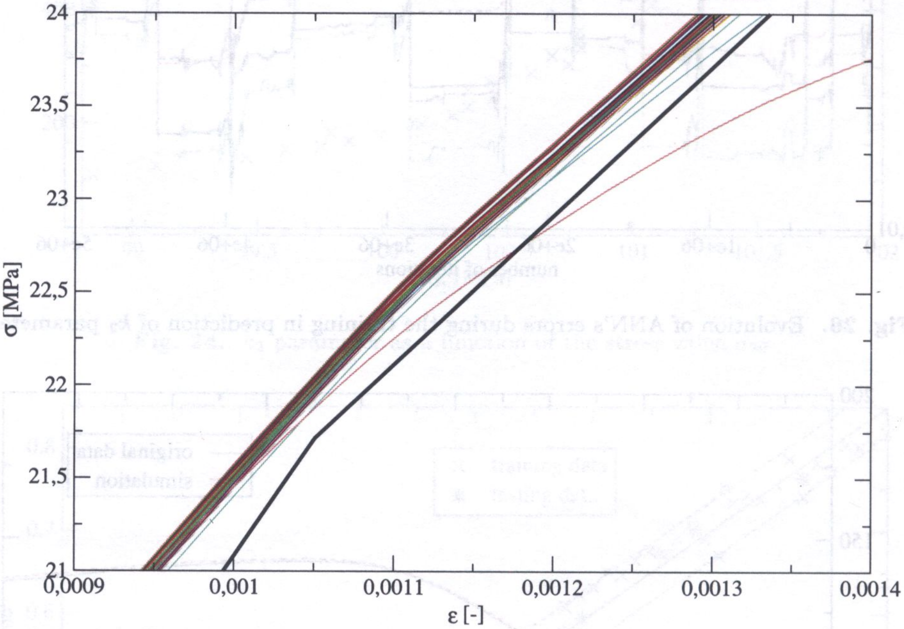

Fig. 28. Bundle of simulated stress–strain curves for uniaxial compression and one (bold black) measured stress–strain curve under zoom

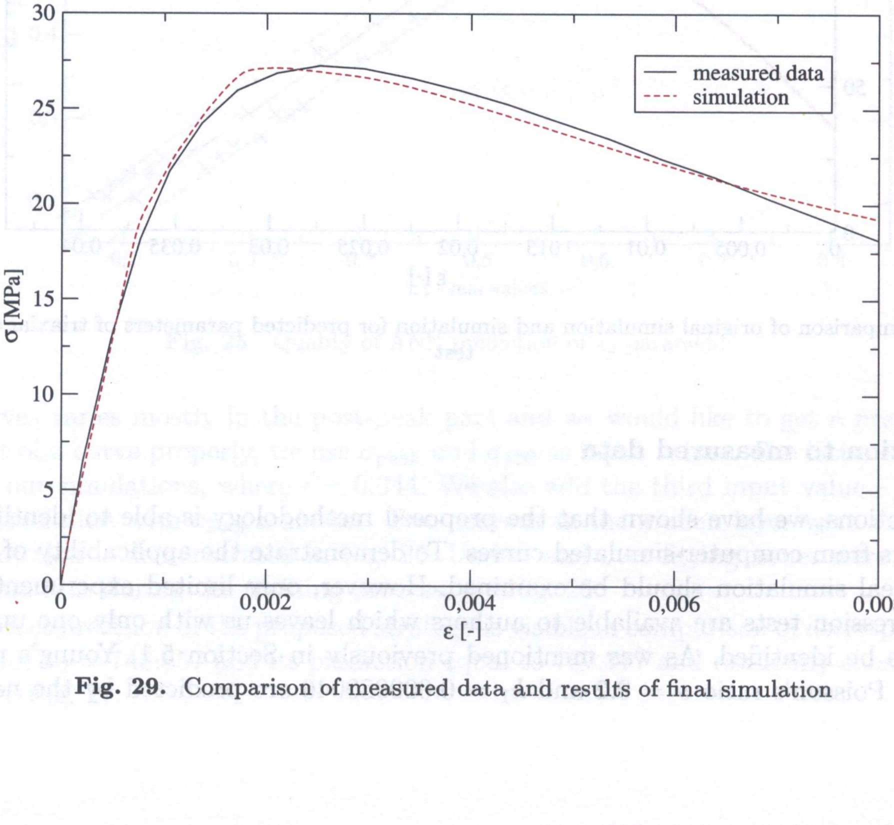

Fig. 29. Comparison of measured data and results of final simulation

6. Conclusion and future work

In the present contribution, an example of the engineering problem, which is difficult to be solved by traditional procedures, was solved using methods of soft computing. Particularly, an artificial neural network was used to estimate required microplane material model parameters. As the training procedure, the genetic algorithm-based method **GRADE** was used. A number of needed simulations is reduced by the application of the Latin Hypercube Sampling method. The sensitivity analysis shows not only the influence of individual parameters but also approximately predicts the errors produced by the neural network.

Table 7. Final status of M4 identification project

Parameter	Test	ANN's topology
E	Uniaxial compression	3 + 2 + 1
ν	Uniaxial compression	4 + 3 + 1
k_1	Uniaxial compression	4 + 2 + 1
k_2	Triaxial loading	3 + 2 + 1
k_3	Hydrostatic loading	5 + 3 + 1
k_4	Hydrostatic loading	3 + 2 + 1
c_3	×	×
c_{20}	Uniaxial compression	3 + 2 + 1

Results of our contribution, see Table 7, confirm the claims made by authors [2] of the microplane M4 model on individual parameters fitting. Only the parameter c_3 remains undetermined but the parameter c_3 should be almost constant for the wide range of concretes and our computations confirm almost zero impact of this parameter on stress–strain curves.

The rather severe disadvantage of the microplane model, and also of the proposed methodology, is an extreme demand of computational time. A suite of 30 uniaxial tests consumes approximately 25 days on a single processor PC with the Pentium IV 3400 MHz processor and 3 GB RAM. If we run tests in parallel on 7 computers, the needed time is less than 4 days. The hydrostatic and triaxial tests are less demanding, by running in parallel on 7 computers the required time is less than one day for each test. Although several neural networks were created to avoid the time-consuming numerical analysis, the proposed methodology still needs to compute 30 uniaxial tests to properly identify c_{20} parameter and a set of 30 hydrostatic and triaxial tests to fit k_3 , k_4 and k_2 . This drawback will be the subject of future work.

Acknowledgments

We would like to express our thanks to David Lehký and Drahomír Novák, Technical University of Brno, for numerous suggestions and inspiring discussions. This work was supported by CEZ MSM 6840770003 project.

References

[1] Z.P. Bažant, F.C. Caner. Microplane model M5 with kinematic and static constraints for concrete fracture and anelasticity. Part I: Theory, Part II: Computation. *Journal of Engineering Mechanics-ASCE*, **131**(1): 31–40, 41–47, 2005.

[2] Z.P. Bažant, F.C. Caner, I. Carol, M.D. Adley, S.A. Akers. Microplane model M4 for concrete. Part I: Formulation with work-conjugate deviatoric stress, Part II: Algorithm and calibration. *Journal of Engineering Mechanics – ASCE*, **126**: 944–953, 954–961, 2000.

[3] J. Drchal, A. Kučerová, J. Němeček. Using a genetic algorithm for optimizing synaptic weights of neural networks. *CTU Reports*, **7**(1): 161–172, 2003.

[4] O. Hrstka, A. Kučerová. Improvements of real coded genetic algorithms based on differential operators preventing the premature convergence. *Advances in Engineering Software*, **35**(3-4): 237–246, 2004.

[5] A. Ibrahimbegović, C. Knopf-Lenoir, A. Kučerová, P. Villon. Optimal design and optimal control of structures undergoing finite rotations and elastic deformations. *International Journal for Numerical Methods in Engineering*, **61**(14): 2428–2460, 2004.

[6] R.L. Iman, W.J. Conover. Small sample sensitivity analysis techniques for computer models with an application to risk assessment. *Communications in Statistics, Part A - Theory and Methods*, **9**(17): 1749–1842, 1980.

[7] M. Jirásek, Z.P. Bažant. *Inelastic Analysis of Structures.* John Wiley and Sons, 2001.

[8] J. Němeček, Z. Bittnar. Experimental investigation and numerical simulation of post-peak behavior and size effect of reinforced concrete columns. *Materials and Structures*, **37**(267): 161–169, 2004.

[9] J. Němeček, P. Padevět, B. Patzák, Z. Bittnar. Effect of transversal reinforcement in normal and high strength concrete columns. *Materials and Structures*, **38**(281): 665–671, 2005.

[10] J. Němeček, B. Patzák, D. Rypl, Z. Bittnar. Microplane models: computational aspects and proposed parallel algorithm. *Computers and Structures*, **80**(27-30): 2099–2108, 2002.

[11] D. Novák. *FREET:Feasible Reliability Engineering Efficient Tool.* Brno University of Technology, Faculty of Civil Engineering, Institute of Structural Mechanics, Praha, Czech Republic, 2002. Web page: http://www.freet.cz

[12] D. Novák, D. Lehký. ANN inverse analysis based on stochastic small-sample training set simulation. *Engineering Applications of Artificial Intelligence, Special issue on Engineering Applications of Neural Networks — Novel Applications of Neural Networks in Engineering*, **19**(7): 731–740, 2006.

[13] B. Patzák, Z. Bittnar. Design of object oriented finite element code. *Advances in Engineering Software*, **32**(10-11): 759–767, 2001. Web page: http://www.oofem.org

[14] A. Strauss, K. Bergmeister, D. Novák, D. Lehký. Stochastische Parameteridentifikation bei Konstruktionsbeton für die Betonerhaltung, *Beton- und Stahlbetonbau*, **99**(12): 967–974, 2004.

[15] L.H. Tsoukalas, R.E. Uhrig. *Fuzzy and neural approaches in engineering.* John Wiley and Sons, 1997.